metals

MDPI

Article

An Investigation of the Mechanical, Thermal and Electrical Properties of an AA7075 Alloy Reinforced with Hybrid Ceramic Nanoparticles Using Friction Stir Processing

Ahmed B. Khoshaim [1], Essam B. Moustafa [1,*], Mashhour A. Alazwari [1] and Mohammed A. Taha [2]

[1] Mechanical Engineering Department, Faculty of Engineering, King Abdulaziz University, Jeddah P.O. Box 80204, Saudi Arabia
[2] Solid State Physics Department, National Research Centre, El Buhouth St., Dokki 12622, Egypt
* Correspondence: abmostafa@kau.edu.sa

Abstract: Aluminum AA7075, graphene nanoplates (GNP), boron nitride (BN), and vanadium carbide (VC) are used to fabricate hybrid nanocomposite matrices. BN and VC serve as secondary reinforcement particles in the fabrication of hybrid composites, with graphene (GNP) as a key component of the hybrid process. Friction stir processing (FSP) was used to manufacture the composite matrix; it also has a major role in improving the microstructure's grain refinement, as well as the reinforcing of the particles, which play a crucial role in limiting grain growth during the dynamic recrystallization process. Consequently, the grain sizes of the nanocomposite AA7075/GNPs, hybrid composites AA7075/GNPs+BN, and hybrid composites AA7075/GNPs+BN+VC were decreased by an average of 10.3 times compared to the base alloy. The SEM analysis demonstrated that the dispersion of the hybrid reinforcement particles was performed, and the particles were dispersed uniformly throughout the metal matrix. The mechanical characteristics of the hybrid AA7075/GNPs+BN+VC include the highest compression stress and hardness values due to the homogeneity of the hybridization process between the BN and VC particles. The GNPs reduce the electrical conductivity by 7.3% less than the base alloy. In comparison, when hybridized with BN and VC, it is reduced by 24.4% and 31.1%, respectively. In addition, the inclusion of thermally insulating materials, such as BN and VC, decreases the thermal conductivity of the hybrid composite metal matrices.

Keywords: hybrid composite; thermal conductivity; industrial development; friction stir processing; GNPs; mechanical properties

Citation: Khoshaim, A.B.; Moustafa, E.B.; Alazwari, M.A.; Taha, M.A. An Investigation of the Mechanical, Thermal and Electrical Properties of an AA7075 Alloy Reinforced with Hybrid Ceramic Nanoparticles Using Friction Stir Processing. *Metals* **2023**, *13*, 124. https://doi.org/10.3390/met13010124

Academic Editor: Manoj Gupta

Received: 6 December 2022
Revised: 3 January 2023
Accepted: 6 January 2023
Published: 8 January 2023

1. Introduction

Aluminum, one of the most widely used metals in the world, is found in large quantities. Aluminum composites and aluminum alloys are used in various industries, including automotive, military, and nuclear (for neutron absorption) [1,2], due to their high modulus of elasticity, strength, and resistance to wear, creep, and fatigue. Aluminum matrix composites (also called AMCs), reinforced with advanced ceramic and non-ceramic particles, are becoming increasingly popular as a unique potential structural material that can be used in a wide range of lightweight applications [3–6]. However, there are some limitations to using these composites because the inclusion of some reinforcements reduces their hardness and ductility [7–9]. While maintaining the SiC concentration, graphite is used as a reinforcement for the material, with aluminum as the base metal. Heat treatment has been shown to increase the wear resistance of aluminum matrix composites, in addition to other parameters [10]. As the amount of fly ash in AA 6063 alloy increased, the wear decreased when the load was increased [11]. The size and distribution of second-phase particles during precipitation hardening are two of the most crucial aspects to consider when altering the microstructural properties to induce superplastic behavior. FSP determined that the superplastic behavior in 7075-T651 was due to the movement of grain

boundaries. As a result, as the operating temperature rises, the stress concentration at the grain boundaries decreases [12]. The process parameters' impact on particle dispersion and grain refinement in AA 7075/SiC/CB hybrid composites produced through stir casting with FSP as a secondary process was investigated [13]. The coarse grains included in the casting are refined and equiaxed in this step.

Fracture tests conducted on the composite material showed that it experienced ductile cracking, with pits forming on the fracture surface. The load was transferred to the reinforced particles through a pull-out process, demonstrating strong interfacial bonding between the components. Although the FSP composite had almost twice the strength of the cast substrate, it maintained its ductility [14]. Multiple passes of overlapping FSP were used to create titanium nanohydroxyapatite (nHA) nanocomposites. After five passes, the nHA particles were dispersed evenly throughout the titanium matrix. After being refined in SZ, the initially rough crystal structure became finely equiaxed, and flaws such as holes were not observed [15]. AZ31 magnesium alloy was strengthened by adding Ti6Al4V particles to the mix at a volumetric range of 27%. The grain size and structure improved as the reinforcing particle content increased [16]. Ti6Al4V particles were evenly dispersed and chemically bound to the matrix alloy and interface, with no diffusion layer, reaction layer, or porosity found.

Moreover, it was noted that the composites were enhanced upon adding Ti6Al4V particles, which also led to sufficient plastic flow before fracture. Ti6Al4V/Ag nanocomposites, which FSP produces, have been shown to strengthen the mechanical characteristics and surface biocompatibility. The rotation of the FSP instrument is mainly responsible for the streamlining and streaking distribution of Ag nanoparticles seen following FSP [17]. The addition of reinforcing particles increases the hardness of the surface composite; many authors reported that the reinforcement affects the behavior of the composite surface against the scratch effect [18–22]. SiC was used to reinforce Al 1050/Al 5052 alloys; thus, the ARB approach was used to manufacture a multilayered composite through six passes using FSP [23]. Although the reinforcement particles vary, some effective particles, when embedded in an aluminum–metal matrix, improve their hardness properties; moreover, the surface of the hybrid composites increases the mechanical and hardness behavior [24–26]. A 5% graphite and 2%, 4%, 6%, and 8% Al_2O_3 were used to fabricate the Al 7075/Al_2O_3/graphite hybrid composite. The hardness, tensile strength, flexural strength, and compressive strength of Al 7075/Al_2O_3/graphite hybrid composites increase with the ceramic phase weight [27]. According to the aforementioned literature review, hybrid surface composites on alloys in the Al 7-xxx series range have increased microhardness, wear resistance, and ballistic characteristics [28]. However, these composites' tensile or compression behavior has not yet been the subject of any prominent investigations. BN and VC nanoparticles are used as auxiliary components in the fabrication of hybrid composites, with GNPs serving as the main component of the hybrid process. The main objective of the present study is to determine the effect of GNPs, when hybridized with heavy ceramic particles, on the physical and mechanical properties. Therefore, in the current investigation, AA 7075 wrought alloy is reinforced by mono and hybrid reinforcement particles using a friction stir process; thus, the compression, yield stress, and elastic modulus are studied. Furthermore, the thermal and electrical conductivities are measured to show the effect of the reinforcement particles on the composite matrices.

2. Materials and Methods

The base matrix of this work was AA 7075 aluminum alloy; hence, Table 1 lists the chemical composition of the utilized sheet. The particles that are used to reinforce and improve the AA7075 aluminum base matrix are BN nanoparticles with an average particle size of 160 ± 32 nm and a purity of 99%. The particles were obtained from Shanghai Runwu Chemical Technology Co., Ltd., Shanghai, China. The graphene flake powder (GNP) consisted of a single layer (0.3–1.0 nm average), with a particle size of 130 ± 25 nm; the vanadium carbides had an average particle size of 1.12 ± 0.31 μm and 99% purity. GNP

(50 volume%) + BN (50 volume%) hybrid and triple hybrid GNP (33.33 volume%) + BN (33.3 volume%) + VC (33.33 volume%). Transmission electron microscopy (TEM) was used to characterize the reinforcement particles (JEOL JSM-200F, Tokyo, Japan). The micro- and nanostructures of the reinforcing particles are depicted in Figure 1 (GNP, VC, and BN). The FSP technique was used to fabricate the hybrid composite surface by adding the hybrid reinforcement particles in the pre-processed holes in the AA7075 surfaces, as shown in Figure 2a. The hybrid reinforcement particles were thoroughly mixed for homogenization before they were filled into the holes. The FSP was carried out at a tool rotation speed of 1120 rpm, a traveling speed rate of 30 mm/minute, and a tilt angle of 2°. The FSP tool is shown in Figure 2c and was designed according to [27]. After the FSP, samples were cut to obtain information about the microstructure, mechanical properties, and physical properties. For microstructural analysis, the as-received and fabricated composites were mechanically ground with SiC paper, polished, and then etched with standard metallurgical agents. JEOL scanning electron microscopy was used for the analysis of the microstructure.

Table 1. Chemical composition of AA 7075 wrought alloy (wt%).

Si	Fe	Cu	Mn	Mg	Cr	Zn	Ti	Others Total	Al
0.4	0.5	1.7	0.3	2.6	0.19	5.8	0.2	0.15	Remainder

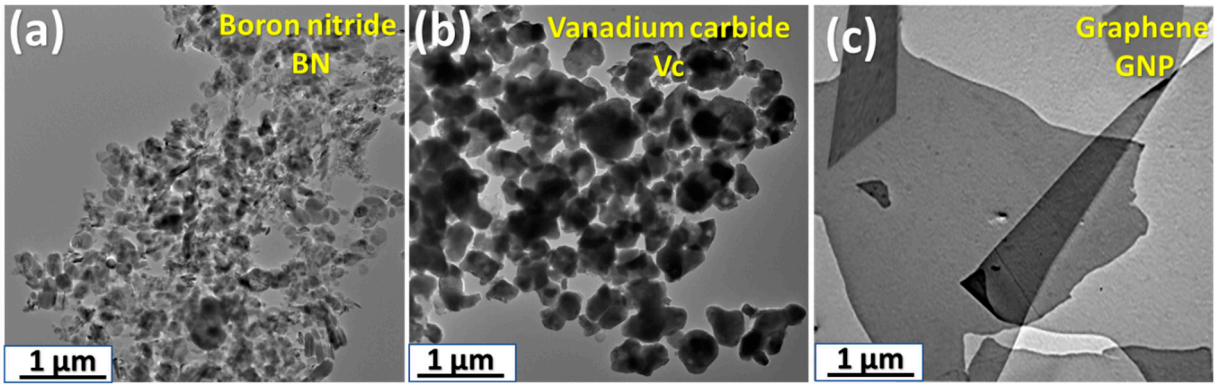

Figure 1. TEM images of the reinforcement particles: (**a**) hexagonal boron nitride nanopowder, (**b**) vanadium carbide particles, (**c**) graphene nanoplate.

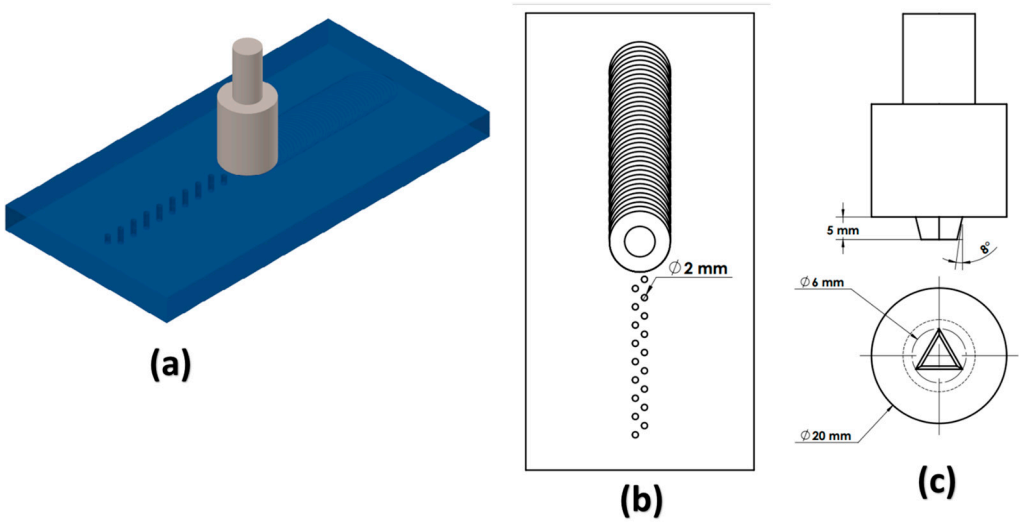

Figure 2. Schematic drawing of the FSP process: (**a**) 3D model of the fabrication process, (**b**) hole design in the AA7075 plate, (**c**) FSP tool design.

According to the ASTM E-384-17 standard, Vickers micro-hardness tests were performed. The readings were taken across the sample surface in all processing regions to create the hardness profile. The hardness of the processed region was measured using Vickers microhardness test equipment with a 1 kg load and a 10 s dwell time. Eight measurements were obtained close to each zone, and the mean results were analyzed and discussed further. Before the microhardness test, the samples were surface-cleaned and polished. In addition, the indenter took eight measurements along the sample's surface using 1 mm increments. The compression test was carried out in accordance with the guidelines outlined in ASTM E 9–89a for Metallic Materials Conducted at Room Temperature. Three samples were used in each experiment, and their averages were then determined.

Armfield linear heat conduction was used to test thermal conductivity. Based on Fourier's law, the heat flow equation can be used to compute the sample's conductivity coefficient, K (W/m·k) [28]. The device consists of a heating element, an electrically heated source, an intermediate stage, tested samples, and a cooling water supply. All three components are radially insulated to reduce losses and direct heat transfer. A tested sample is attached to the intermediate part using a thermal conductivity material and coated with an insulating substance to prevent heat loss. Then, we clamp the intermediate part between the heated and cooled regions. Therm paste was applied to all surfaces to ensure complete contact and effective thermal exchange between components. Timing the collection of 500 mL water samples per 20 s adjusted the cooling water supply flow to 1.5 L/min. The heater heated the cylinder. A calibrated substance in contact with the heated part transfered heat linearly to the sample. The cooling water supply cooled the sample. Steady-state thermal conductivity was measured directly. Fourier's law controls the sample's heat transfer rate, and heat flow is one-dimensional, as shown in Equation (1).

$$Q = -kA\frac{dT}{dX} \tag{1}$$

In this equation, Q represents the x-direction heat transfer rate, k represents the thermal conductivity of the sample material, A represents the x-normal cross-sectional area of the sample, and dT/dX is the x-direction temperature gradient. The heating element receives the electric power determined by Equation (2).

$$P_{in} = V{\cdot}I \tag{2}$$

Thus, P_{in} is the watt input, V is the volts, and I is the amps flowing through the heater. Under the assumption of zero heat loss, Equation (3) is used to determine the direction and rate of heat transmission through the sample (3). Considering that heat conduction only happens along a single axis, Equation (4) is obtained. As the last step, we use Equation (5) to determine k, the thermal conductivity. We consider the temperature gradient over the thickness of the sample ΔX, denoted by T.

$$Q = P_{in} \tag{3}$$

$$Q = kA\frac{\Delta T}{\Delta X} \tag{4}$$

$$k = \frac{Q/A}{\frac{\Delta T}{\Delta X}} \tag{5}$$

The electrical conductivity was measured at room temperature. The compression test was conducted at an ambient temperature of 25 °C. Measurements were made according to ASTM D-4496, and the samples were prepared for the measurement process; hence, the tested samples had dimensions of 10 mm × 10 mm × 3 mm.

3. Results and Discussion

3.1. Microstructure

As-received AA 7075 alloy was examined using optical microscopy to calculate the mean grain size, which was observed to be 206.89 ± 76 µm. Figure 3a shows the elongated grains before subjecting the sheets to the FSP process. At the same time as it causes significant plastic deformation in the stirred zone (SZ), the FSP also generates tremendous heat in the SZ. In such a zone, the dynamic recrystallization process is performed due to the stirring action of the FSP. Therefore, the SZ comprises more homogeneous, equiaxed, and refined grains than the base metal (BM). The SZ grains have a size distribution closer to the mean than those in the as-received alloy, showing the homogeneity of the grain size. The reinforcing particles (BN and VC) considerably impact the refined grain shape and microstructure. Therefore, the grains grow finely and more uniform once the particles are strengthened. During the dynamic recrystallization process, the nanoparticles inhibit grain growth development, resulting in refined grains. According to [29–31], the presence of reinforcement nanoparticles in the matrix enhances the viscosity of the processed metal during FSP; this mechanism improves the solubility and aids in the uniformity and dispersion of the various particles in the composite matrix. Figure 3b–d show the refined and equiaxed grains as a result of stirring action; the average grain size of the fabricated composites AA7075/GNPs, AA7075/GNP+BN, and AA7075/GNPs+BN+VC was 22.64 + 2.35 µm, 19.58 + 1.56 µm, and 19.04 + 1.52 µm, respectively. The enhancement in grain refinement reached approximately 10.5-fold less than the base alloy size.

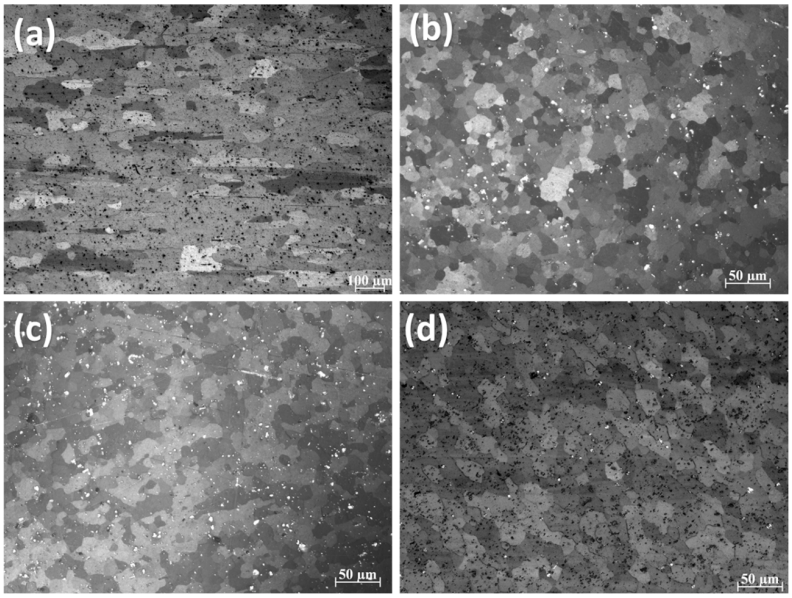

Figure 3. Optical microstructure images of the investigated composites: (**a**) AA7075 wrought alloy, (**b**) monocomposite AA7075/GNPs, (**c**) hybrid composite AA7075/GNP+BN, (**d**) hybrid composite AA7075/GNP+BN+VC.

Figure 4 shows SEM pictures of the prepared and polished surfaces of mono and hybrid composite metal matrices of AA7075 wrought alloy reinforced by GNPs, BN, and VC, and the hybrid composite (AA7075/GNPs+BN+VC). The SEM photos show the dispersion of GNPs, BN, and VC particles in the friction-stirred zone (SZ), where they were scanned. The distribution and dispersion of GNPs, BNs, and VCs in the mono and hybrid composite metal matrices were uniform and homogeneous. The SEM analysis of hybrid AA7075/GNP+BN+VC and EDS mapping analysis was conducted to evaluate the reinforcements' distribution and the unfavorable agglomeration and nanocluster impact of reinforcing ceramic particles. EDS maps indicated the existence of reinforced particles in the SZ and the studied alloy's primary alloying elements and phases, as shown in Figure 5.

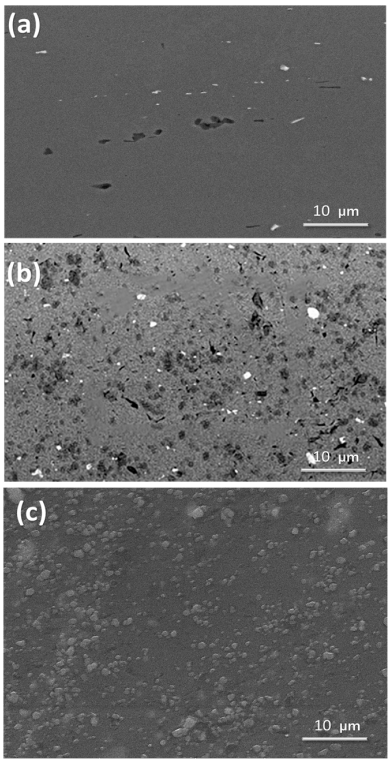

Figure 4. SEM images: (**a**) monocomposite AA7075/GNPs, (**b**) hybrid composite AA7075/GNP+BN, (**c**) hybrid composite AA7075/GNP+BN+VC.

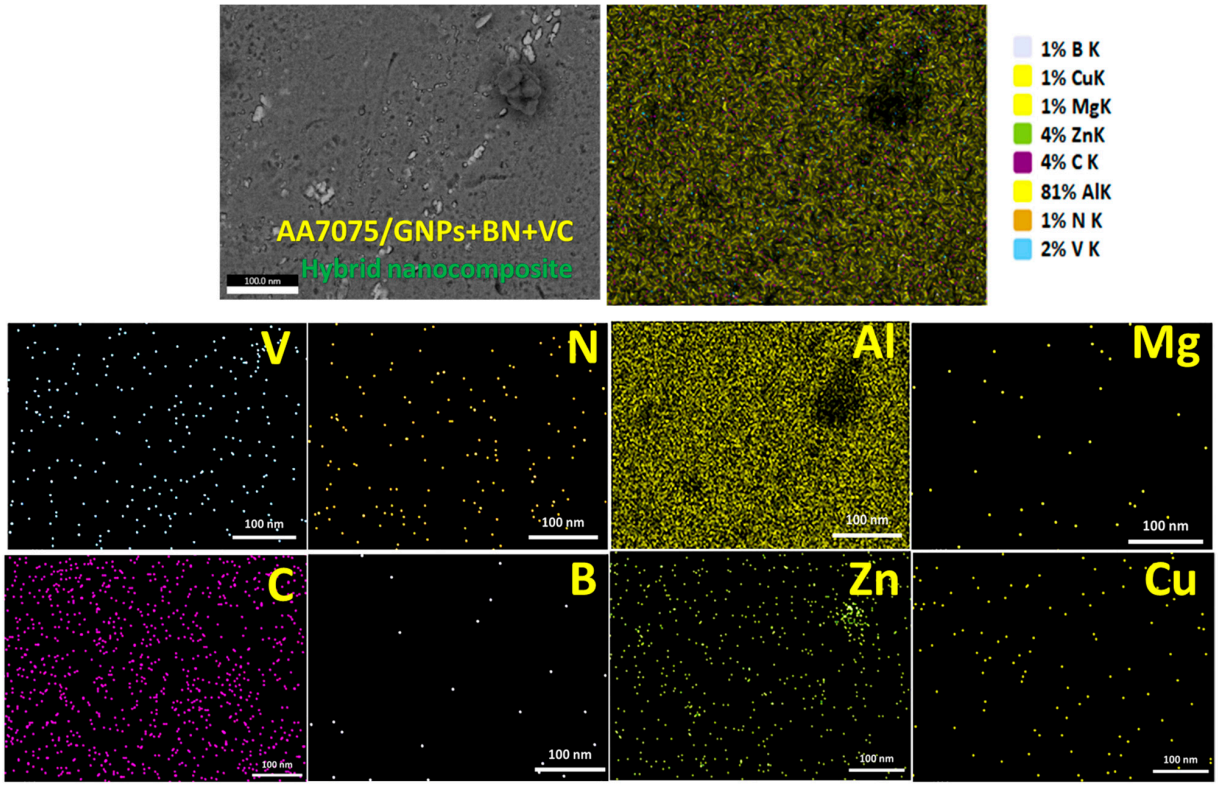

Figure 5. EDS mapping images of the hybrid composite AA7075/ GNP+BN+VC.

In general, it was noted that the triple reinforcing nanoparticles were uniformly distributed in the SZ, with no significant clustering seen. Adding GNP nanoparticles

improves the mechanical characteristics and gives the hybrid composite sufficient strength. Incorporating large particles, such as VC, into the production of hybrid composites during the FSP process increases the composite's strength and grain refinement. This process may be attributed to grain refinement, which depends on the availability of nucleation sites in the matrix and the concentrations of reinforcement particles, which rise with larger additions of various reinforcement particle sizes.

3.2. Thermal Conductivity

Figure 6 illustrates the heat conductivity of the investigated metal matrix composites. Based on the findings, it was determined that the wrought AA7075 alloy has higher thermal conductivity than the investigated composites due to the absence of the particles that impede the heat conductivity flow from the source to the received temperature sensor, in addition to being associated with large grains with fewer grain boundaries. This is mostly due to the presence of free electors. A significant amount of weight is given to the arrangement of the molecules in terms of the lattice component. The values of "k" are lowered with reinforced metal matrix composites and VC ceramic particles; as a result, the "k" value for the hybrid composite is reduced by 0.75%; the result is consistent with [32]. This may be explained by the poor thermal conductivity of VC, which results in the material having a value that ranges from 22 to 40 W/m.K. On the other hand, GNP particles boost the thermal conductivity, as was shown in the monocomposite AA 7075/GNPs, where the thermal conductivity increased by 15% more than the base alloy. The higher thermal conductivity value (178 W/m.K.) may be traced back to the GNPs as the source of the improved thermal conductivity. Although there are GNPs present in the hybrid matrix, the total thermal conductivity of the surface composite is lowered since the h-BN has low thermal conductivity, which leads to reduced resultant thermal conductivity. BN nanoparticles' effect on the resulting composite is to reduce the fabricated composite's thermal conductivity; hence, it has a low BN value of 30 W/m.K. Moreover, it causes a lubricating action during the stirring process.

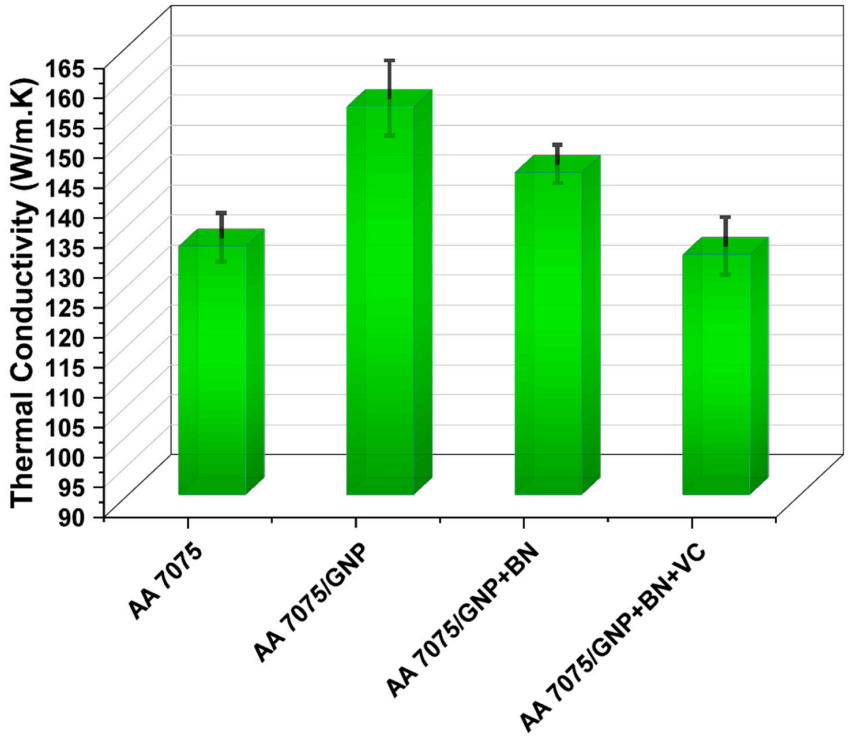

Figure 6. Thermal conductivity of the base alloy AA7075, fabricated monocomposite AA7075/GNPs, and hybrid composite matrices.

3.3. Mechanical Properties

The compressive strength of the AA7075/GNP+BN+VC hybrid composite has the maximum value; hence, it increased to 317.83 MPa. Compared to the triple additive, the composites that did not contain VC-reinforced particles exhibited lower compressive stress. As a result, the compressive stresses of the base material AA7075, the monocomposite AA7075/GNPs, and the hybrid composite AA7075/GNPs+BN were measured at 247.1 MPa, 257.5 MPa, and 278.8 MPa, respectively, as shown in Figure 7. There is a discernible impact on the mechanical characteristics brought about by the hybridization of ceramic particles. The compression results show that the ultimate compressive strength (UCS) increases with the addition of reinforcing particles. The GNPs have little effect compared to the reinforcing particles BN and VC. The addition of boron increased the UCS value by up to 14% compared to the base metal. Hybridization with vanadium carbide led to a significant improvement in the UCS value to 32.5%. The remarkable improvement in the AA7075/GNP+BN+VC hybrid composite is due to the homogenization and good distribution of the reinforcing particles used in the hybrid process of aluminum alloy. In addition, the grain is refined during the FSP.

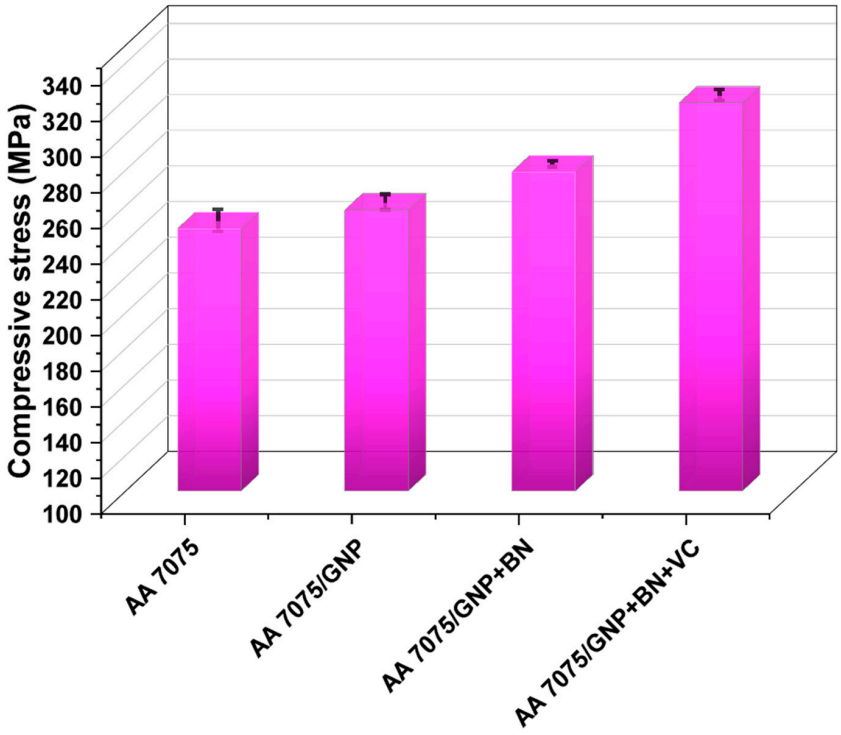

Figure 7. Ultimate compressive stress.

3.4. Hardness Behavior

Figure 8 shows the Vickers microhardness profile for the materials studied. As a result, the hardness of the manufactured samples was examined throughout the stirred zone (SZ), heat-affected zone (HAZ), and base metal. The microhardness profile of the analyzed samples demonstrates that the base metal AA7075 has a lower value than the hybrid AA7075/GNP+BN+VC. The hybrid has the highest hardness value in the stirred zone. The hardness of the AA7075/GNP+BN hybrid nanocomposite is midway between that of the base alloy and that of the triple hybrid nanocomposites. It was logical to predict that better granule refinement would result in a higher FSP hardness in the presence of ceramic particles. There is a minor increase in hardness in the hardened (HAZ) region owing to heat action on the grains induced by the tool's shoulder. Figure 9 shows the average hardness in the stirred zone for several investigated composites. According to the Hall–Petch connection, the grain size of a metallic substance impacts its mechanical

characteristics, particularly its strength and hardness. According to the same theory, the rise in hardness values may be attributed to a decrease in grain structure caused by the friction stirring process and particle dispersion during the fabrication of freshly made aluminum composites [33]. The microhardness value of the surface composites is increased due to the grain-refining impact of dispersed GNPs with BN and VC particles, and the grain size of the AA7075 aluminum alloy surface hybrid composites in the stirring zone is smaller than that of the base alloy. The microhardness values of the AA7075/GNP composites were 12.1% and 21%, and were greatly improved in the AA7075/GNP+BN+VC composites. The hardness improvement may be attributed to the alloy matrix's refining activity, which resulted in the uniform dispersion of hard nanoceramics within the matrix.

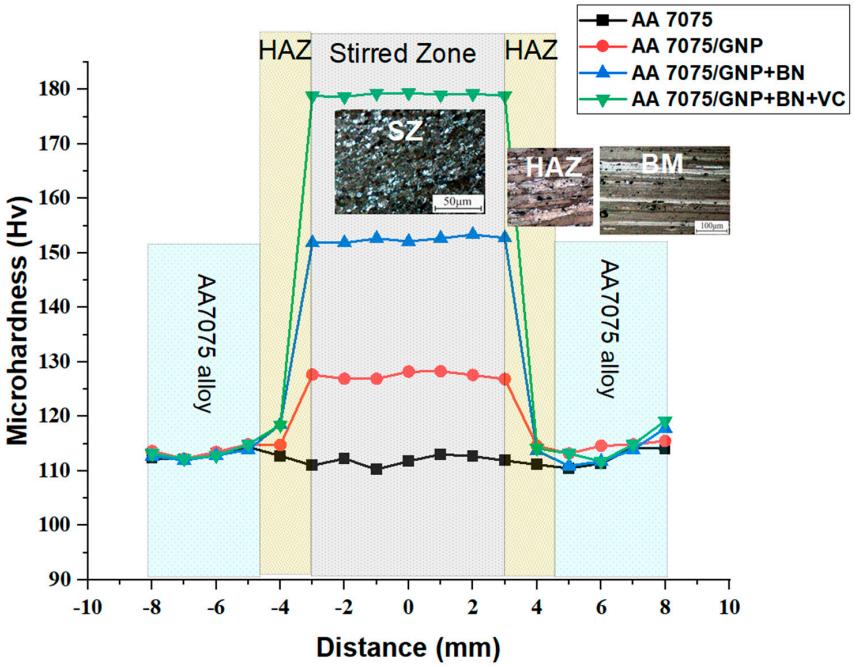

Figure 8. Microhardness profile of the investigated samples through stirred zone (SZ), heat-affected zone (HAZ), and base metal (BM).

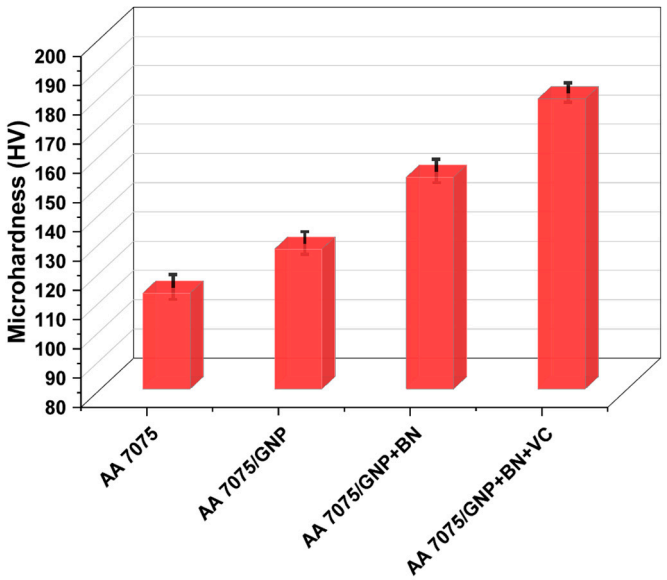

Figure 9. Average microhardness values at the center of the stirred zone of the different metal matrix composites.

3.5. Electrical Conductivity

Figure 10 shows the effect of additional hybrid reinforcement on AA 7075 alloy by the FSP method. The results show that the aluminum alloy's electrical conductivity decreased after adding different hybrid reinforcements. However, the GNPs exhibit good electrical conductivity compared with the other investigated hybrid reinforcements. Lower electrical conductivity may be associated with lower conductivity for reinforcements such as BN and VC, compared to the AA7075 alloy. Moreover, the decrease in the conductivity of composites can be attributed to internal electron movement, where hybrid ceramic reinforcements increase the number of scattering sites for conduction electrons [34,35]. It is also worth mentioning that the conductivity of the AA7075/GNP composite is greater than that of the hybrid composites GNP+BN and GNP+BN+VC because BN and VC are insulating materials and the results were consistent with [36,37].

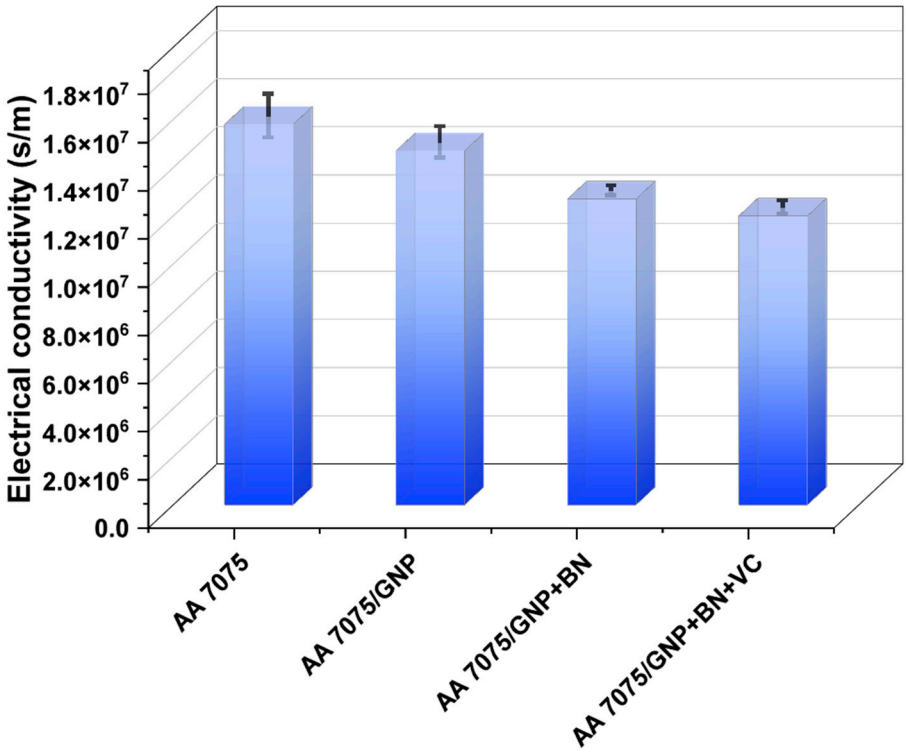

Figure 10. The electrical conductivity of the investigated alloy and fabricated composites.

4. Conclusions

Hybrid nanocomposite matrices were obtained using ceramic reinforcing particles and aluminum AA7075 as an aluminum alloy. In order to create hybrid nanocomposites, GNPs were used as the fixed component of the hybridization process, with BN nanoparticles and VC particles acting as complementary particles.

The microstructure of the metal matrix grain was improved using the FSP approach, which is crucial for limiting grain development during the dynamic recrystallization process. As a consequence, the grain size of the AA7075 base alloy was decreased from 206.89 µm to an average of 20 µm for the majority of mono and hybrid nanocomposite matrices. According to the SEM study, the hybrid reinforcement particles were successfully dispersed and uniformly distributed throughout the metal matrix.

The mechanical properties of the hybrid AA7075/GNP+BN+VC included the maximum compression strength and hardness value; hence, this can be attributed to the homogenization of the hybridization process of vanadium carbide with boron nitride. Both have different, distinct mechanical properties that enhance the properties of the resulting hybrid composite. The electrical conductivity of aluminum alloys decreases with the hybridization

process, especially in the presence of BN and VC particles, due to impediments to the movement of electrons within the composite matrix. Hence, the AA7075/GNP, GNP+BN, and GNP+BN+VC composites are decreased by 7.5%, 24.5%, and 31.7%, respectively, compared to the base alloy.

The thermal conductivity of the monocomposite AA7075/GNP is increased by 15% more than the as-received base alloy; on the other hand, the hybrid composite metal matrices were affected by the lower thermal conductivity due to the presence of thermally insulating elements such as BN and VC.

Author Contributions: Conceptualization, A.B.K. and E.B.M.; methodology, E.B.M.; validation, M.A.T. and M.A.A.; formal analysis, A.B.K.; investigation, E.B.M.; resources, A.B.K.; data curation, M.A.A.; writing—original draft preparation, E.B.M.; writing—review and editing, E.B.M.; supervision, A.B.K.; project administration, A.B.K.; funding acquisition, M.A.A. All authors have read and agreed to the published version of the manuscript.

Funding: This research was funded by The Deanship of Scientific Research (DSR) at King Abdulaziz University (KAU), grant number "G:191-135-1443" and The APC was funded by authors.

Data Availability Statement: Not applicable.

Acknowledgments: The Deanship of Scientific Research (DSR) at King Abdulaziz University (KAU), Jeddah, Saudi Arabia, funded this project (G: 191-135-1443).

Conflicts of Interest: The authors declare no conflict of interest.

References

1. Abenojar, J.; Velasco, F.J.; Martinez, M.A. Optimization of processing parameters for the Al+10% B4C system obtained by mechanical alloying. *J. Mater. Process. Technol.* **2007**, *184*, 441–446. [CrossRef]
2. Tyagi, L.; Butola, R.; Jha, A.K. Mechanical and tribological properties of AA7075-T6 metal matrix composite reinforced with ceramic particles and aloevera ash via Friction stir processing. *Mater. Res. Express* **2020**, *7*, 066526. [CrossRef]
3. Thangarasu, A.; Murugan, N.; Dinaharan, I.; Vijay, S.J. Microstructure and microhardness of AA1050/TiC surface composite fabricated using friction stir prcessing. *Sadhana* **2012**, *37*, 579–586. [CrossRef]
4. Wu, B.; Ibrahim, M.; Raja, S.; Yusof, F.; Razak, B.B.A.; Bin Muhamad, M.R.; Huang, R.; Zhang, Y.; Badruddin, I.A.; Hussien, M.; et al. The influence of reinforcement particles friction stir processing on microstructure, mechanical properties, tribological and corrosion behaviors: A review. *J. Mater. Res. Technol.* **2022**, *20*, 1940–1975. [CrossRef]
5. Moustafa, E.B. Hybridization effect of BN and Al2O3 nanoparticles on the physical, wear, and electrical properties of aluminum AA1060 nanocomposites. *Appl. Phys. A* **2021**, *127*, 1–9. [CrossRef]
6. Ahmadi, M.; Rahmatabadi, D.; Pahlavani, M.; Marzbanrad, J.; Hashemi, R.; Afkar, A. Experimental study of the defects, mechanical and microstructural characteristics of friction-stir-welded Al 6061 sheets. *Surf. Topogr. Metrol. Prop.* **2021**, *9*, 035012. [CrossRef]
7. Miracle, D. Metal matrix composites—From science to technological significance. *Compos. Sci. Technol.* **2005**, *65*, 2526–2540. [CrossRef]
8. Moustafa, E.B.; Alazwari, M.A.; Abushanab, W.S.; Ghandourah, E.I.; Mosleh, A.O.; Ahmed, H.M.; Taha, M.A. Taha Influence of Friction Stir Process on the Physical, Microstructural, Corrosive, and Electrical Properties of an Al–Mg Alloy Modified with Ti–B Additives. *Materials* **2022**, *15*, 835. [CrossRef] [PubMed]
9. Moustafa, E.B.; Abushanab, W.S.; Melaibari, A.; Mikhaylovskaya, A.V.; Abdel-Wahab, M.S.; Mosleh, A.O. Nano-Surface Composite Coating Reinforced by Ta2C, Al2O3 and MWCNTs Nanoparticles for Alu-minum Base via FSP. *Coatings* **2021**, *11*, 1496. [CrossRef]
10. Naveed, M.; Khan, A.R.A. Dry sliding wear of heat treated hybrid metal matrix composites. *IOP Conf. Series Mater. Sci. Eng.* **2016**, *149*, 012084. [CrossRef]
11. Kumar, D.; Singh, P.K. Investigation of wear characteristics of Al-4032 based metal matrix composite using Taguchi's optimization approach. *Mater. Res. Express* **2019**, *6*, 106543. [CrossRef]
12. Patel, V.V.; Badheka, V.; Kumar, A. Influence of Friction Stir Processed Parameters on Superplasticity of Al-Zn-Mg-Cu Alloy. *Mater. Manuf. Process.* **2016**, *31*, 1573–1582. [CrossRef]
13. Rana, H.; Badheka, V.; Kumar, A.; Satyaprasad, A. Strategical parametric investigation on manufacturing of Al–Mg–Zn–Cu alloy surface composites using FSP. *Mater. Manuf. Process.* **2018**, *33*, 534–545. [CrossRef]
14. Roy, P.; Singh, S.; Pal, K. Enhancement of mechanical and tribological properties of SiC- and CB-reinforced aluminium 7075 hybrid composites through friction stir processing. *Adv. Compos. Mater.* **2017**, *28*, 1–18. [CrossRef]
15. Rahmati, R.; Khodabakhshi, F. Microstructural evolution and mechanical properties of a friction-stir processed Ti-hydroxyapatite (HA) nanocomposite. *J. Mech. Behav. Biomed. Mater.* **2018**, *88*, 127–139. [CrossRef]

16. Dinaharan, I.; Zhang, S.; Chen, G.; Shi, Q. Assessment of Ti-6Al-4V particles as a reinforcement for AZ31 magnesium alloy-based composites to boost ductility incorporated through friction stir processing. *J. Magnes. Alloy* **2021**, *10*, 979–992. [CrossRef]
17. Wang, L.; Xie, L.; Shen, P.; Fan, Q.; Wang, W.; Wang, K.; Lu, W.; Hua, L.; Zhang, L.-C. Surface microstructure and mechanical properties of Ti-6Al-4V/Ag nanocomposite prepared by FSP. *Mater. Charact.* **2019**, *153*, 175–183. [CrossRef]
18. Moustafa, E.B.; Melaibari, A.; Alsoruji, G.; Khalil, A.M.; Mosleh, A.O. Tribological and mechanical characteristics of AA5083 alloy reinforced by hybridising heavy ceramic particles Ta2C & VC with light GNP and Al2O3 nanoparticles. *Ceram. Int.* **2021**, *48*, 4710–4721. [CrossRef]
19. Moustafa, E.B.; Melaibari, A.; Basha, M. Wear and microhardness behaviors of AA7075/SiC-BN hybrid nanocomposite surfaces fabricated by friction stir processing. *Ceram. Int.* **2020**, *46*, 16938–16943. [CrossRef]
20. Jain, V.K.; Yadav, M.K.; Siddiquee, A.N.; Khan, Z.A. Fabrication of surface composites on different aluminium alloys via friction stir process—A review report. *Aust. J. Mech. Eng.* **2022**, 1–24. [CrossRef]
21. Moustafa, E.B.; Elsheikh, A.H.; Taha, M.A. The effect of TaC and NbC hybrid and mono-nanoparticles on AA2024 nanocomposites: Microstructure, strengthening, and artificial aging. *Nanotechnol. Rev.* **2022**, *11*, 2513–2525. [CrossRef]
22. Moustafa, E.B.; Abushanab, W.S.; Melaibari, A.; Yakovtseva, O.; Mosleh, A.O. The Effectiveness of Incorporating Hybrid Reinforcement Nanoparticles in the Enhancement of the Tribological Behavior of Aluminum Metal Matrix Composites. *Jom* **2021**, *73*, 4338–4348. [CrossRef]
23. Deng, H.; Chen, Y.; Jia, Y.; Pang, Y.; Zhang, T.; Wang, S.; Yin, L. Microstructure and mechanical properties of dissimilar NiTi/Ti6Al4V joints via back-heating assisted friction stir welding. *J. Manuf. Process.* **2021**, *64*, 379–391. [CrossRef]
24. Ghandourah, E.I.; Moustafa, E.B.; Hussein, H.; Mosleh, A.O. The Effect of Incorporating Ceramic Particles with Different Morphologies on the Microstructure, Mechanical and Tribological Behavior of Hybrid TaC_ BN/AA2024 Nanocomposites. *Coatings* **2021**, *11*, 1560. [CrossRef]
25. Kök, M.; Özdin, K. Wear resistance of aluminium alloy and its composites reinforced by Al2O3 particles. *J. Mater. Process. Tecnol.* **2007**, *183*, 301–309. [CrossRef]
26. Veeramallu, K.; Sunkari, S.; Mishikari, N. Experimental investigation on microstructure and mechanical properties of functionally graded AA7075 using friction stir processing. *Mater. Today Proc.* **2022**, *56*, 1551–1557. [CrossRef]
27. Baradeswaran, A.; Perumal, A.E. Study on mechanical and wear properties of Al 7075/Al2O3/graphite hybrid com-posites. *Compos. Part B Eng.* **2014**, *56*, 464–471. [CrossRef]
28. Patil, N.A.; Pedapati, S.R.; Mamat, O.B. A Review on Aluminium Hybrid Surface Composite Fabrication Using Friction Stir Processing. *Arch. Metall. Mater.* **2020**, *65*, 441–457.
29. Emamian, S.; Awang, M.; Yusof, F.; Hussain, P.; Mehrpouya, M.; Kakooei, S.; Moayedfar, M.; Zafar, A. A Review of Friction Stir Welding Pin Profile. In Proceedings of the 2nd International Conference on Mechanical, Manufacturing and Process Plant Engineering, Kuala Lumpur, Malaysia, 23–24 November 2016; Springer: Cham, Switzerland, 2017; pp. 1–18.
30. Greene, G.A. *Heat Transfer, in Encyclopedia of Physical Science and Technology*, 3rd ed.; Meyers, R.A., Ed.; Academic Press: New York, NY, USA, 2003; pp. 279–292.
31. Goodarzi, M.; Toghraie, D.; Reiszadeh, M.; Afrand, M. Experimental evaluation of dynamic viscosity of ZnO–MWCNTs/engine oil hybrid nanolubricant based on changes in temperature and concentration. *J. Therm. Anal. Calorim.* **2018**, *136*, 513–525. [CrossRef]
32. Saeedi, A.H.; Akbari, M.; Toghraie, D. An experimental study on rheological behavior of a nanofluid containing oxide nanoparticle and proposing a new correlation. *Physica E* **2018**, *99*, 285–293. [CrossRef]
33. Zadeh, A.D.; Toghraie, D. Experimental investigation for developing a new model for the dynamic viscosity of sil-ver/ethylene glycol nanofluid at different temperatures and solid volume fractions. *J. Therm. Anal. Calorim.* **2017**, *131*, 1449–1461. [CrossRef]
34. Aziz, S.S.A.; Abulkhair, H.; Moustafa, E.B. Role of hybrid nanoparticles on thermal, electrical conductivity, microstructure, and hardness behavior of nanocomposite matrix. *J. Mater. Res. Technol.* **2021**, *13*, 1275–1284. [CrossRef]
35. Thapliyal, S.; Dwivedi, D.K. Barium titanate reinforced nickel aluminium bronze surface composite by friction stir processing. *Mater. Sci. Technol.* **2017**, *34*, 366–377. [CrossRef]
36. Al-Mosawi, B.T.; Wexler, D.; Calka, A. Characterization and mechanical properties of α-Al2O3 particle reinforced aluminium matrix composites, synthesized via uniball magneto-milling and uniaxial hot pressing. *Adv. Powder Technol.* **2017**, *28*, 1054–1064. [CrossRef]
37. AbuShanab, W.S.; Moustafa, E.B.; Ghandourah, E.; Taha, M.A. Effect of graphene nanoparticles on the physical and mechanical properties of the Al2024-graphene nanocomposites fabricated by powder metallurgy. *Results Phys.* **2020**, *19*, 103343. [CrossRef]